Journal of Zhejiang University-SCIENCE A (Applied Physics & Engineering) *2024 25(7):586-595*
www.jzus.zju.edu.cn; www.springer.com/journal/11582
E-mail: jzus_a@zju.edu.cn

Research Article

https://doi.org/10.1631/jzus.A2300159

Evolution mechanism and quantitative characterization of initial micro-cracks in marble under triaxial compression

Zhiliang WANG[1]✉, Songyu LI[1], Jianguo WANG[2], Ao LI[1], Weixiang WANG[1], Chenchen FENG[1], Jingjing FU[1]

[1]*School of Civil Engineering, Hefei University of Technology, Hefei 230009, China*
[2]*School of Mechanics and Civil Engineering, China University of Mining and Technology, Xuzhou 221116, China*

Abstract: The initial micro-cracks affect the evolution characteristics of macroscopic deformation and failure of rock but are often ignored in theoretical calculation, numerical simulation, and mechanical experiments. In this study, we propose a quantitative analysis model to investigate the effects of initial micro-cracks on the evolution of marble deformation and failure. The relationship between the micro-crack propagation and the marble failure characteristics was comprehensively studied by combining theoretical analysis with a micro-computed tomography (micro-CT) scanning technique. We found that with the increase of confining pressure, the matrix elastic modulus of the marble first increased and then tended to be stable, while the micro-cracks increased exponentially. The sensitivity ranges of the marble sample matrix elastic modulus and micro-cracks to confining pressure were 0–30 MPa and 30–50 MPa, respectively. The porosity and Poisson's ratio decreased exponentially. The increasing proportion of internal micro-cracks led to an increase in the sample non-uniformity. The samples presented mainly shear failure under triaxial compression, and the failure angle decreased linearly with the increase of confining pressure. The convergence direction of cracks decreased gradually. This quantitative analysis model could accurately portray the relationship between the overall macroscopic deformation and the deviatoric stress of the samples at the compaction and the linear elastic stages, thus deepening the understanding of the stress–strain behavior of rocks.

Key words: Marble; Initial micro-cracks; Triaxial compression; Constitutive relationship; Crack evolution

1 Introduction

As the shallow mineral geological resources around the world are on the verge of exhaustion, the depth of underground mining is increasing year by year and mining conditions are becoming increasingly complex (Chen, 2017; Xie, 2019). Due to the compound effects of geological conditions (such as tectonic stress, and plate and shell movement) and human activities (such as the disturbance of shield excavation and blasting mining vibration) (Li et al., 2015; Liu et al., 2019; Wang et al., 2022), numerous micro-cracks become randomly distributed in the underground engineering rock mass (Liu and Dai, 2021). Micro-cracks can cause difficulties in deep geotechnical engineering support and frequent geological disasters, including roof collapse, rockburst, and coal (gas) outbursts as a result of unstable deformation of rock mass structure (Zhang and Zhao, 2014). Such disasters can be regarded as the result of the generation and propagation of rock cracks. Therefore, the accurate characterization of mechanical properties and crack evolution in rocks under different loading conditions is of great significance for evaluating the structural stability of deep underground engineering.

The rock mass is an important component of an underground engineering structure. It is a natural heterogeneous material that includes rock matrix and micro-cracks (pores) (Nur, 1971; Morgan et al., 2013). The random distribution of micro-cracks in the rock matrix determines the internal structural characteristics of rock and affects its physical and mechanical properties. Zuo et al. (2019) studied the growth of cracks in rocks under different confining pressures and temperatures. They derived a crack growth model for triaxial compression and verified their model with experimental results.

✉ Zhiliang WANG, cvewzL@hfut.edu.cn
Zhiliang WANG, https://orcid.org/0000-0001-9989-3109
Songyu LI, https://orcid.org/0000-0002-8884-3226

Received Mar. 26, 2023; Revision accepted Apr. 23, 2023;
Crosschecked Nov. 21, 2023; Online first Jan. 13, 2024

Zhang et al. (2020) abstracted brittle rock materials into skeletons and cracks, and established a constitutive model to consider the initial pore closure effect with the instantaneous strain and statistical damage theory.

The stress–strain relationship is fundamental for the stress and deformation analysis of rocks (Chang and Lee, 2004) and has been studied under various loadings and environments. Bieniawski (1967) summarized the stage of sample stress–strain curves through rock mechanics experiments. He pointed out that different occurrence states of micro-cracks in a sample corresponded to different characteristic stresses. Zhao and Liu (2012) used Hooke's law based on the natural strain and engineering strain to describe the deformation of internal pores and other parts of porous rock, respectively. Peng et al. (2016) pointed out that the proportion of initial micro-cracks in rocks could be regarded as the initial micro-crack damage.

The above studies have analyzed the stress–strain relationship of rocks in the pre-peak stage, but have rarely quantitatively analyzed the proportion of initial micro-cracks and the evolution of mechanical characteristics with confining pressure. The relationship between the crack growth and macroscopic failure characteristics of the rock sample under triaxial compression has also not been fully discussed. In this study, a theoretical model for the quantitative analysis of the initial proportion of micro-cracks of rock was first established based on the stress decomposition of triaxial compression. Then, the model was verified against experimental data. Finally, the fracture evolution characteristics of the loaded rock samples were analyzed with micro-computed tomography (micro-CT) scanning. The results can provide reference parameters for the numerical simulation when the initial micro-cracks and the rock matrix are modeled separately.

2 Model establishment

Dynamic and static tests showed that the mechanical properties of deformation and failure of a rock were closely related to the micro-crack propagation in the rock. The increasing slope of the stress–strain curve also changes gradually with the growth of micro-cracks. The pre-peak stage of the stress–strain curve can be roughly divided into three stages (Corkum and Martin, 2007), based on the slope change (Fig. 1), where σ_{cc} and σ_{ci} are the stress at the end of compaction point and the crack initiation stress, respectively. σ_p is the peak stress; E_s is the elastic modulus of the sample; σ is the stress; ε is the strain; j is any point on the compaction and linear elastic stages of the stress–strain curve, and ε_j and σ_j are the corresponding strain and stress values, respectively; ε_{P1} and ε_{P2} are the partial strains of the matrix and cracks, respectively.

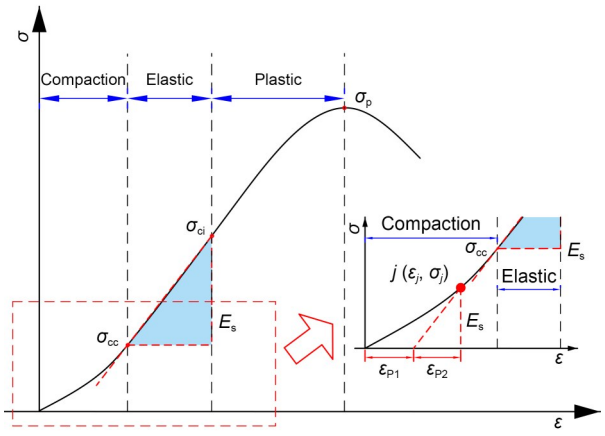

Fig. 1 Deformation stage of pre-peak stress–strain curves of rock

The stress–strain relationship in the compaction stage is closely related to the volume of initial micro-cracks. When a sample is loaded to the crack closure stress, the initial micro-cracks inside the sample are basically closed, and the slope of the stress–strain curve does not change. The slope of the corresponding position curve is the elastic modulus E_s of the sample. Therefore, the initial micro-cracks can be quantitatively characterized by the stress–strain relationship during the compaction and the linear elastic stages.

Natural rock can be regarded as a composite rock with a matrix and micro-cracks (pores). The contribution of micro-crack deformation to the overall macroscopic deformation of rock can be analyzed using the effective medium theory (Cai et al., 2017). As shown in Fig. 1, the strain ε of rock at the compaction and linear elastic stages has two components: the partial strain ε_{P1} of the matrix and the partial strain ε_{P2} of the cracks:

$$\varepsilon = \varepsilon_{P1} + \varepsilon_{P2}. \tag{1}$$

Introducing the proportion of initial micro-cracks in the rock, the axial partial strains of the matrix and cracks are given by:

$$\varepsilon_{\mathrm{P1}}=\left(1-\frac{V_{\mathrm{C}}}{V}\right)\varepsilon_{\mathrm{mz}}, \tag{2}$$

$$\varepsilon_{\mathrm{P2}}=\frac{V_{\mathrm{C}}}{V}\varepsilon_{\mathrm{cz}}, \tag{3}$$

where V_{C} is the initial micro-crack volume in the sample; V is the overall volume of the sample; $\varepsilon_{\mathrm{mz}}$ is the axial strain of the matrix; $\varepsilon_{\mathrm{cz}}$ is the axial strain of the micro-cracks.

The overall macroscopic strain of the sample is the summation of the two components expressed as

$$\varepsilon=\left(1-\frac{V_{\mathrm{C}}}{V}\right)\varepsilon_{\mathrm{mz}}+\frac{V_{\mathrm{C}}}{V}\varepsilon_{\mathrm{cz}}. \tag{4}$$

The slope variation of the stress–strain curve of rock samples at the compaction and the linear elastic stages shows that when the sample is loaded to the crack closure stress, the micro-cracks inside the sample are basically closed, and the stress–strain relationship is approximately linear and follows the generalized Hooke's law as

$$\varepsilon_{\mathrm{mz}}=\frac{1}{E_{\mathrm{m}}}\left[\sigma_z-\mu_{\mathrm{m}}(\sigma_x+\sigma_y)\right], \tag{5}$$

where E_{m} and μ_{m} are the elastic modulus and Poisson's ratio of the rock matrix, respectively. σ_x, σ_y, and σ_z are the principal stresses.

The sampling process of the representative volume element (RVE) is shown in Fig. 2.

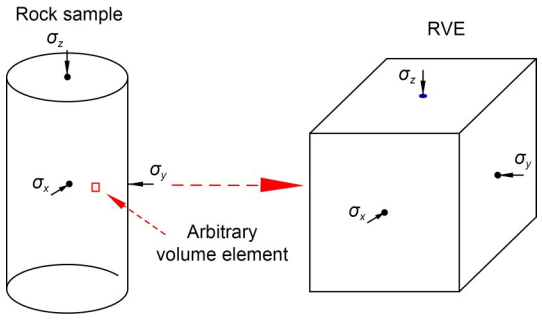

Fig. 2 Sampling process of RVE

First, the stress environment at the sampling site should be considered in the mechanical test and the result analysis of the rock sample. Then, the rock sample is assumed to be an aggregate (n equal parts), and one micro-element (the arbitrary volume element) is taken for analysis. An RVE (Fig. 3) is taken to characterize

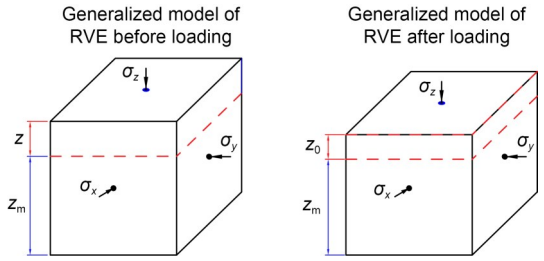

Fig. 3 Conception and deformation of RVE in the sample

the deformation characteristics of rock under the external load, where z_{m} is the equivalent matrix; z and z_0 are the equivalent micro-crack lengths before and after loading, respectively.

The axial strain of the micro-element after loading can be expressed as

$$\mathrm{d}\varepsilon_{\mathrm{cz}}=\frac{z-z_0}{z}. \tag{6}$$

The deformation of the micro-cracks inside rock is different from that of the matrix. The micro-cracks in natural rocks are randomly distributed in the matrix. At present, it is technically unrealistic to measure the strain field borne by micro-cracks. Natural strain can describe this part of deformation more accurately (Freed, 1995). Combined with the above analysis, the deformation of an equivalent micro-crack unit is described by natural strain as

$$\mathrm{d}\varepsilon_{\mathrm{cz}}=\int_z^{z_0}\left(-\frac{\mathrm{d}z}{z}\right)=-\ln\frac{z_0}{z}. \tag{7}$$

Combining Eqs. (6) and (7) gives:

$$\frac{z_0}{z}=\mathrm{e}^{-\mathrm{d}\varepsilon_{\mathrm{cz}}}. \tag{8}$$

In the RVE, the deformation of micro-cracks is assumed to follow the generalized Hooke's law (Xie et al., 2022) as

$$\mathrm{d}\varepsilon_{\mathrm{cz}}=\frac{1}{E_{\mathrm{c}}}\left[\mathrm{d}\sigma_z-\mu_{\mathrm{c}}(\mathrm{d}\sigma_x+\mathrm{d}\sigma_y)\right], \tag{9}$$

where E_{c} and μ_{c} are the elastic modulus and Poisson's ratio of the rock with micro-cracks, respectively.

Therefore, the strain increment is obtained based on Eqs. (6), (8), and (9) as

$$\mathrm{d}\varepsilon_{\mathrm{cz}}=1-\mathrm{e}^{-\frac{1}{E_{\mathrm{c}}}[\mathrm{d}\sigma_z-\mu_{\mathrm{c}}(\mathrm{d}\sigma_x+\mathrm{d}\sigma_y)]}. \tag{10}$$

The strain of the internal initial micro-cracks is then expressed as

$$\varepsilon_{\mathrm{P2}}=\int_{i=1}^{n}\mathrm{d}\varepsilon_{\mathrm{cz}}, \tag{11}$$

or

$$\varepsilon_{\mathrm{P2}}=\int_{i=1}^{n}\frac{V_{\mathrm{b}}}{nV_0}\left(1-\mathrm{e}^{-\int_{i=1}^{n}\frac{1}{E_{\mathrm{c}}}[\mathrm{d}\sigma_z-\mu_{\mathrm{c}}(\mathrm{d}\sigma_x+\mathrm{d}\sigma_y)]}\right)=\frac{V_{\mathrm{C}}}{V}\left(1-\mathrm{e}^{-\frac{1}{E_{\mathrm{c}}}[\sigma_z-\mu_{\mathrm{c}}(\sigma_x+\sigma_y)]}\right), \tag{12}$$

where V_0 is the volume of the RVE and V_{b} is the volume of the micro-cracks in the RVE.

Combining Eqs. (4), (5), and (12) obtains the quantitative analysis model of initial micro-cracks as

$$\varepsilon=\left(1-\frac{V_{\mathrm{C}}}{V}\right)\frac{1}{E_{\mathrm{m}}}\left[\sigma_z-\mu_{\mathrm{m}}(\sigma_x+\sigma_y)\right]+\frac{V_{\mathrm{C}}}{V}\left(1-\mathrm{e}^{-\frac{1}{E_{\mathrm{c}}}[\sigma_z-\mu_{\mathrm{c}}(\sigma_x+\sigma_y)]}\right). \tag{13}$$

Each parameter in this equation has clear physical significance but is difficult to measure directly using conventional rock mechanics methods and experiments. They can be calculated indirectly through the stress–strain relationship of rock under triaxial compression.

In the conventional triaxial compression test (confining pressure $\sigma_3=\sigma_x=\sigma_y$), the test process is to firstly increase the confining pressure to a preset value, and then apply the axial stress. At this time, the stress applied to the sample is the deviatoric stress ($\sigma_z-\sigma_x$). That is, the experimental results monitored by the triaxial compression device measure the relationship between the deviatoric stress and the sample strain. Through stress decomposition, the stress state of the triaxial compression sample can be decomposed into the compound action of hydrostatic pressure and deviatoric stress (Fig. 4). The uniaxial compression is a special case of triaxial compression ($\sigma_x=\sigma_y=0$ MPa).

The above stress decomposition shows that the strain of rock obtained by a conventional triaxial compression experiment is due to the deviatoric stress. Therefore, the quantitative analysis model of the initial micro-cracks inside the sample can be expressed as

$$\varepsilon_{\mathrm{T}}=\left(1-\frac{V_{\mathrm{C}}}{V}\right)\frac{1}{E_{\mathrm{m}}}(\sigma_z-\sigma_x)+\frac{V_{\mathrm{C}}}{V}\left(1-\mathrm{e}^{-\frac{\sigma_z-\sigma_x}{E_{\mathrm{c}}}}\right), \tag{14}$$

where ε_{T} is the axial strain of the sample under triaxial compression.

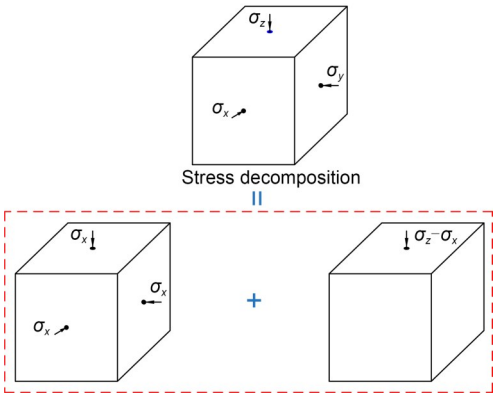

Fig. 4 Load stress decomposition of conventional triaxial compression sample

3 Results

3.1 Model validation

To verify this proposed model, a series of triaxial tests were carried out on marble samples, and further details of the tests are given in Section S1 of the electronic supplementary materials (ESM). The deviatoric stress axial strain curve of a triaxial compression marble sample is shown in Fig. 5a.

The above analysis showed that the initial micro-cracks of the sample can be quantitatively characterized through the compaction and the linear elastic stages of the stress–strain curve. Therefore, it was necessary to quantitatively determine the segment points of the linear elastic stage. Comparative analysis was conducted on the stress distribution at characteristic points (e.g., $\sigma_{\mathrm{ccd}}=\sigma_{\mathrm{cc}}-\sigma_3$) of the marble triaxial compression samples in this study. Combined with the acoustic emission monitoring results of crack initiation points in (Zhou et al., 2019), we found that half of the peak deviatoric stress ($0.5\sigma_{\mathrm{pd}}$) of the triaxial compression samples is a definite position point, which is also located in the elastic stage of samples. That is, $0.5\sigma_{\mathrm{pd}}$ is lower than the stress at the crack initiation point σ_{cid} of the sample. Therefore, the analysis range of the above quantitative analysis model for the initial micro-cracks of the samples was [0, $0.5\sigma_{\mathrm{pd}}$], i.e., from

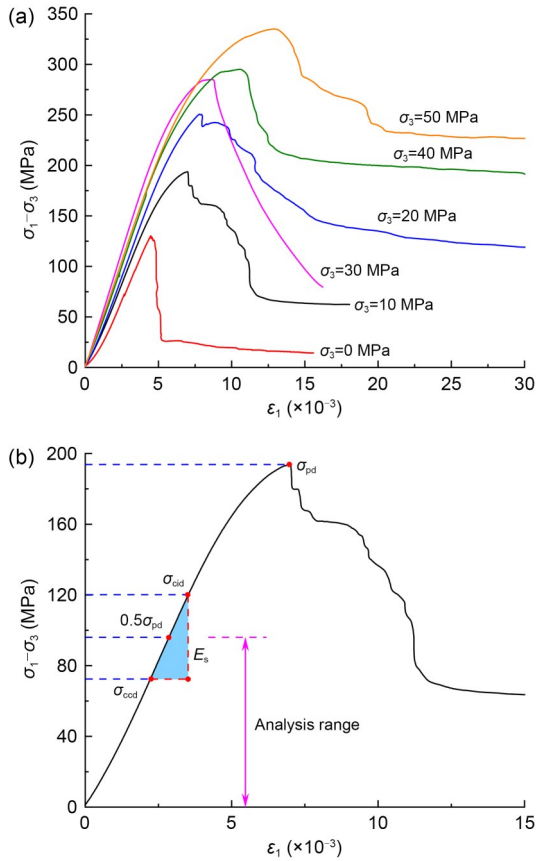

Fig. 5 Deviatoric stress–axial strain curve of triaxial compression marble samples (a) and analysis range of the model (b). σ_1: axial stress of the samples; ε_1: axial strain of the samples; σ_{pd}: peak deviatoric stress; σ_{ccd}: deviatoric stress at the crack closure point; σ_{cid}: deviatoric stress at the crack initiation point

the initial loading point to half of the peak deviatoric stress (Fig. 5b).

Based on the newly established quantitative analysis model, the stress–strain curves of each marble sample under triaxial compression and their corresponding fittings are shown in Fig. 6, taking σ_3=0 MPa as an example. More detailed comparison results can be obtained from Section S2 in the ESM. Under each confining pressure, the results from the micro-cracks quantitative analysis model closely matched the test results (goodness of fit R^2 all greater than 0.9990). The above results indicate that the quantitative analysis model proposed in this study can accurately characterize the relationship between the overall macroscopic deformation and the deviatoric stress in the compaction and the linear elastic stages under triaxial compression. The fitting equations are shown in Eqs. (S1)–(S6) of the ESM.

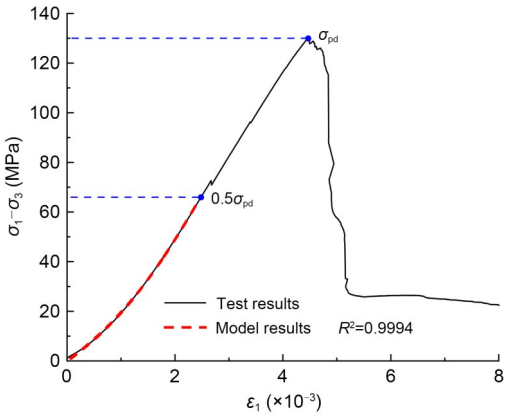

Fig. 6 Comparison between the quantitative crack analysis model curves and marble test results

3.2 Variation of model parameters with confining pressure

The above experimental results show that the initial nonlinear effect gradually decreases with the increase of confining pressure (Fig. 5a). Moreover, the initial stress–strain curves are very close under high confining pressure. This indicates that the confining pressure has a great influence on the degree of closure of the initial micro-cracks in the samples. The parameters for elastic matrix and crack deformation of the marble samples under triaxial compression are shown in Table S1 of the ESM, where the calculation method for Poisson's ratio of the sample μ_s and E_s is from Taheri et al. (2020). E_m is equivalent to E_s.

Table S1 shows that E_c under each confining pressure was numerically three orders of magnitude different from E_m. This verifies the rationality by using the natural strain to describe the micro-crack deformation in the derivation of the above quantitative crack analysis model. Fig. 7 shows the relationship between E_s (calculated in (Taheri et al., 2020)), E_m (calculated using the model in this study), and E_c with confining pressure. Fig. 7a and Table S1 show that E_m and E_s were 36.82 and 33.33 GPa respectively under uniaxial compression (σ_3=0 MPa)–a difference of about 10%. For the samples under triaxial compression (σ_3=10–50 MPa), the difference between E_m and E_s was less than 3%. The above results indicate that E_s was basically the same as E_m, which verifies the correctness of the quantitative crack analysis model. It also shows that our proposed model can be used to calculate E_s. With σ_3 increasing from 0 to 50 MPa, the E_m and E_s of the sample increased at first (σ_3=0–30 MPa) and then tended

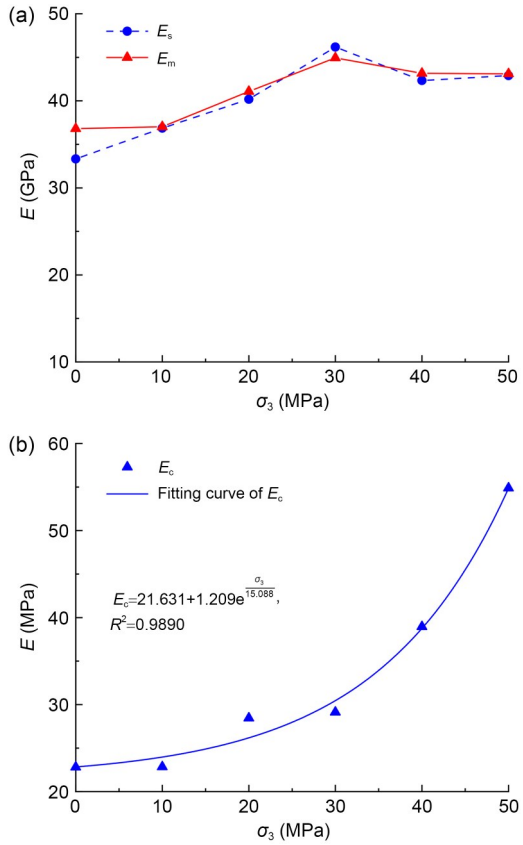

Fig. 7 Influence of the confining pressure σ_3 on sample modulus parameters: (a) sample elastic modulus E_s and matrix elastic modulus E_m; (b) cracks elastic modulus E_c

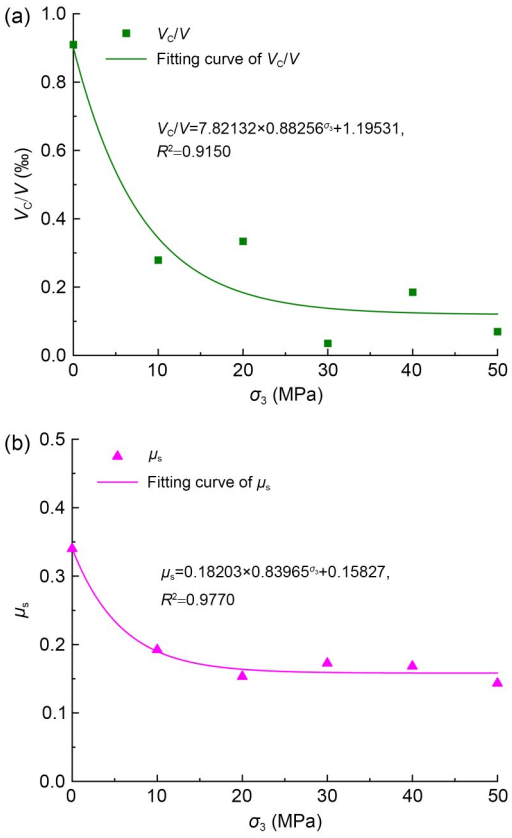

Fig. 8 Variation of porosity V_C/V (a) and Poisson's ratio of the sample μ_s (b) with confining pressure σ_3

to be stable (σ_3=30–50 MPa). E_m was sensitive to σ_3 in the range of 0 to 30 MPa.

Fig. 7b shows the relationship between E_c and σ_3. The results show that with the increase of σ_3, E_c of the samples increases exponentially. The fitting curve is shown in Fig. 7b. E_c increased slowly when σ_3 ranged from 0 to 30 MPa, and increased sharply when it exceeded 30 MPa. The above results demonstrate that the confining pressure for the closure of micro-cracks inside the sample was about 30 MPa. Combined with the results of Fig. 7a, the sensitivity range of E_m to confining pressure was 0–30 MPa, while that of E_c was 30–50 MPa.

Fig. 8 shows the variation of the porosity and Poisson's ratio of samples with confining pressure and the fitting curve. Comparing Fig. 8a with Fig. 7a shows that the variation of porosity is negatively correlated with that of E_s, i.e., when the sample porosity is high, the E_s is correspondingly low. For example, the sample with a confining pressure of 30 MPa has the lowest porosity and the highest elastic modulus. On the whole, an increase of σ_3 will significantly reduce the porosity and μ_s. With the increase of σ_3 from 0 to 50 MPa, the porosity of the sample gradually decreased from 9.10×10^{-4} to 6.96×10^{-5} (Fig. 8a) and μ_s from 0.34 to 0.14 (Fig. 8b). Note that the decrements of porosity and μ_s in the σ_3 range of 0–10 MPa accounted for 75% of the corresponding total decrement when σ_3 increased from 0 to 50 MPa. The existence of σ_3 has a great influence on the porosity and Poisson's ratio.

By comparing the results of Figs. 8a and 8b, the porosity and μ_s decrease gradually with the increase of σ_3 in the same function. The corresponding fitting formulas are shown in Fig. 8. The above results demonstrate that the samples with higher confining pressure are denser, and the circumferential and axial deformation are relatively more synchronous during compression failure (compared with the samples under low confining pressure). The macroscopic deformation of the sample under triaxial compression is closely related to the proportion of micro-cracks inside the sample. The increase of the proportion of micro-cracks will increase the non-uniform deformation of the sample.

3.3 Failure characteristics

The surface failure characteristics are shown in Fig. 9 and the CT scanning sections of the samples in Fig. S3 of the ESM. Fig. 9a and Fig. S3 in the ESM (A3) show that the sample under uniaxial compression (σ_3=0 MPa) had the most surface and internal cracks. The tensile failure is obvious. Comparison of the surface image of the damaged sample with the CT scanning results shows clearly that the CT scanning section image better reveals the propagation of the internal cracks in the sample. According to Figs. 9b–9f and Fig. S3 in the ESM (A6 and A9), the number of surface and internal cracks decreased at first and then increased with confining pressure under triaxial compression (σ_3=10–50 MPa), but it was much lower than that under uniaxial compression. All samples under triaxial compression showed obvious shear failure. The macroscopic failure angle γ between the main macroscopic failure surface and the horizontal plane of each sample is shown in Figs. 9a–9f.

4 Discussion and remarks

4.1 Crack propagation

The failure process of a sample is the propagation process of internal cracks. Combined with the above analysis of the failure characteristic diagrams (Fig. 9 and Fig. S3 in the ESM) of the compressed sample, the evolution of the internal mesoscopic cracks in the compression failure process is qualitatively described in Fig. 10 (Bieniawski, 1967), where σ_{dd} is the damage deviatoric stress of the sample and ε_v is the volumetric strain. In addition, the damage deviatoric stress point is the turning point in dominance from compaction to dilatancy. It is also the division point from stable crack propagation to unstable crack propagation in the sample.

Natural marble samples have micro-cracks (pores) and these initial internal micro-cracks will be gradually closed in response to a continuous external load. As shown in Fig. 10, when an external load was applied to σ_{ccd}, the initial internal micro-cracks were basically closed. With the continuous load, the sample showed obvious elastic deformation characteristics. Therefore, the elastic modulus and Poisson's ratio of the sample were calculated from the data at this stage. When the axial load was applied to σ_{cid}, new cracks began to occur inside the sample, and the elastic deformation characteristics of the sample gradually disappeared.

With the continuous load, the internal cracks continuously expanded (stable expansion stage), and the plastic deformation of the sample gradually appeared. When the axial load was applied to σ_{dd}, the dominant compaction phase of volumetric strain ended and the volumetric strain reached its maximum. After σ_{dd}, the volumetric strain changed to the dilatancy dominated phase, and the volumetric strain continuously decreased. At this stage, the internal cracks began to expand unsteadily and gradually coalesced to form macroscopic cracks (when the axial stress of the sample was near to σ_{pd}). After σ_{pd}, a macroscopic crack plane formed inside the sample and gradually penetrated the outer surface of the sample. From then on, the sample gradually lost its mechanical strength and eventually became unstable and failed.

4.2 Correlation of failure characteristics and crack propagation

In the mesoscopic damage and failure analysis of the loaded rock, non-penetrating micro-cracks in rock samples are generally simplified to circular coin

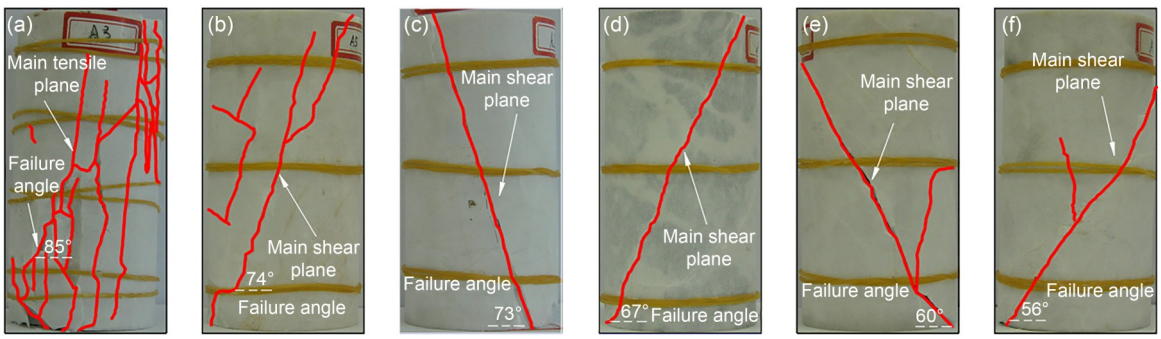

Fig. 9 Failure characteristics of triaxial compression marble samples: (a) σ_3=0 MPa; (b) σ_3=10 MPa; (c) σ_3=20 MPa; (d) σ_3=30 MPa; (e) σ_3=40 MPa; (f) σ_3=50 MPa

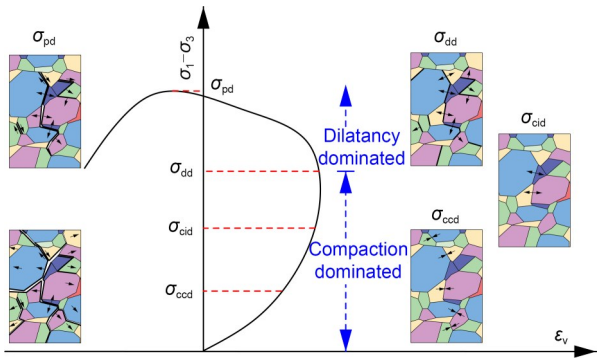

Fig. 10 Sketch of stage evolution characteristics of micro-cracks in samples

cracks or elliptical disk cracks and wing cracks in plane strain analysis (Li XZ et al., 2018; Li SY et al., 2023), as shown in Fig. 11. According to the above analysis, new cracks in marble samples are initiated after the elastic stage (initiation point σ_{cid}). This is because with a continuously increasing load, the crack tip strength factor becomes greater than its critical stress intensity factor, and the internal crack of the sample begins to expand.

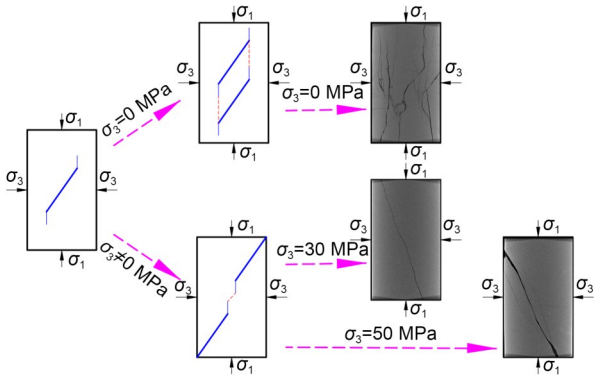

Fig. 11 Mesoscopic crack propagation mode of triaxial compression sample

For the compressed sample, the initiation of internal cracks indicates only the beginning of sample damage and failure. When the internal micro-cracks coalesce with each other (the bridge connection between the cracks), the instability failure of the sample can be observed. Therefore, the propagation mode of the internal cracks in the sample can be described using the connecting process of the double-crack system (Cao et al., 2016).

For marble samples under uniaxial compression, with the increase of axial strain, new tensile cracks occur at the crack tips. Due to the absence of confining pressure, the new cracks spread along the direction parallel to the axial stress, and gradually converge to form a macroscopic tensile failure surface. With the increase of load, the lateral deformation of the macroscopic tensile failure surface continuously increases. When the lateral deformation exceeds the deflection, the tensile failure surfaces will break and connect with each other, resulting in splitting tensile failure of the sample under uniaxial compression.

For a sample under triaxial compression, the confining pressure effectively inhibits the propagation process of internal micro-cracks. Only those cracks parallel to the direction of the deviatoric stress develop. With continuous loading, a number of parallel micro-cracks connect with each other, and finally form a macroscopic shear failure surface through the annular surface of the sample. Therefore, the macroscopic failure angle γ between the macroscopic shear failure surface and the horizontal plane of the sample will gradually decrease with the increase of confining pressure (Fig. 12). There is an obvious linear relationship between γ and σ_3 (goodness of fit R^2=0.9660).

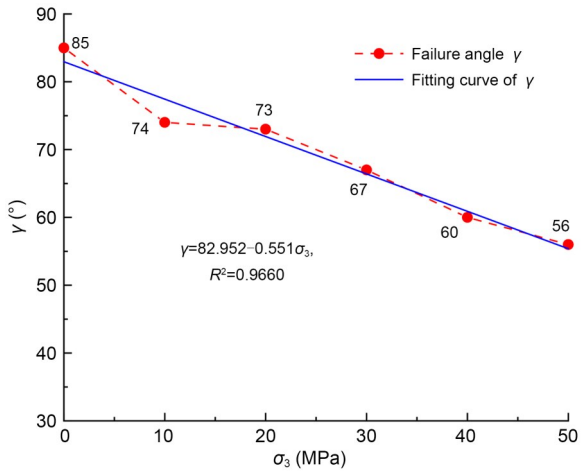

Fig. 12 Variation of γ between the main failure surface and the horizontal plane with confining pressure

The macroscopic failure of the sample is the result of the convergence of cracks. Hence, the propagation direction of the cracks in the sample also linearly decreases with the increase of the confining pressure. In addition, the failure characteristics of samples under triaxial compression of σ_3=50 MPa are different from those under σ_3=30 MPa, showing obvious shear plane damage (Fig. 11). This is because the direction of deviatoric stress on the sample changes with the increase

of confining pressure. The composite action of high confining pressure and axial stress leads to increasing friction between the macroscopic shear planes of the samples, so that the samples with high confining pressure show more severe failure characteristics.

5 Conclusions

A quantitative analysis model was established to represent the initial proportion of micro-cracks in rock. Then, the range of the stress–strain curve was determined for accurate analysis of the initial micro-cracks. This model was verified against the triaxial experimental data. Finally, the evolution of cracks in the loaded samples was revealed using CT scanning images. From these investigations, we drew the following conclusions:

(1) Each parameter in the quantitative analysis model for the initial proportion of micro-cracks in rock has a definite physical meaning. The model can accurately characterize the relationship between the overall macroscopic deformation and the deviatoric stress in both the compaction stage and linear elastic stage under triaxial compression.

(2) The elastic modulus of the matrix first increases and then tends to be stable with the increase of confining pressure, while that of micro-cracks increases exponentially. The sensitivity ranges of the sample matrix elastic modulus and micro-crack elastic modulus to confining pressure are 0–30 MPa and 30–50 MPa, respectively.

(3) The porosity and Poisson's ratio of the sample exhibit an exponential decrease, and the decrements of porosity and Poisson's ratio in the σ_3 range of 0–10 MPa account for 75% of the corresponding total decrement when σ_3 increases from 0 to 50 MPa. The increase of the initial proportion of micro-cracks increases the non-uniform deformation of the sample.

(4) Failure results from the propagation process of micro-cracks. The number of cracks is the highest and the tensile failure characteristics are most obvious in uniaxial compression samples. Shear failure is obvious under triaxial compression. With the increase of confining pressure, the failure angle linearly decreases and the direction of propagation of the internal cracks (corresponding to different expansion modes) also shows a linear decrease.

Acknowledgments

This work is supported by the National Natural Science Foundation of China (Nos. 12272119 and U1965101).

Author contributions

Zhiliang WANG: conceptualization, data processing, writing–review & editing, supervision, and funding acquisition. Songyu LI: conceptualization, data processing, formal analysis, writing–original draft, and writing–review & editing. Jianguo WANG, Ao LI, Weixiang WANG, Chenchen FENG, and Jingjing FU: writing–review & editing.

Conflict of interest

Zhiliang WANG, Songyu LI, Jianguo WANG, Ao LI, Weixiang WANG, Chenchen FENG, and Jingjing FU declare that they have no conflict of interest.

References

Bieniawski ZT, 1967. Mechanism of brittle fracture of rock: parts I, II and III. *International Journal of Rock Mechanics and Mining Sciences & Geomechanics Abstracts*, 4(4): 395-430. https://doi.org/10.1016/0148-9062(67)90030-7

Cai JC, Wei W, Hu XY, et al., 2017. Electrical conductivity models in saturated porous media: a review. *Earth-Science Reviews*, 171:419-433. https://doi.org/10.1016/j.earscirev.2017.06.013

Cao P, Cao RH, Zhao YL, et al., 2016. Propagation-coalescence and rheologic fracture behavior of rock cracks. *The Chinese Journal of Nonferrous Metals*, 26(8):1737-1762 (in Chinese). https://doi.org/10.19476/j.ysxb.1004.0609.2016.08.017

Chang SH, Lee CI, 2004. Estimation of cracking and damage mechanisms in rock under triaxial compression by moment tensor analysis of acoustic emission. *International Journal of Rock Mechanics and Mining Sciences*, 41(7):1069-1086. https://doi.org/10.1016/j.ijrmms.2004.04.006

Chen T, 2017. Study on the Techniques of Active Prevention and Controlling of Rock Burst Based on Controlled Blasting. MS Thesis, Wuhan University, Wuhan, China (in Chinese).

Corkum AG, Martin CD, 2007. The mechanical behaviour of weak mudstone (Opalinus Clay) at low stresses. *International Journal of Rock Mechanics and Mining Sciences*, 44(2):196-209. https://doi.org/10.1016/j.ijrmms.2006.06.004

Freed AD, 1995. Natural strain. *Journal of Engineering Materials and Technology*, 117(4):379-385. https://doi.org/10.1115/1.2804729

Li SY, Wang ZL, Wang JG, et al., 2023. Analysis on mechanical behavior and progressive failure of deep-buried marble based on complete stress-strain curves. *Bulletin of Engineering Geology and the Environment*, 82(4):133. https://doi.org/10.1007/s10064-023-03123-5

Li TC, Lyu LX, Zhang SL, et al., 2015. Development and application of a statistical constitutive model of damaged rock

affected by the load-bearing capacity of damaged elements. *Journal of Zhejiang University-SCIENCE A (Applied Physics & Engineering)*, 16(8):644-655. https://doi.org/10.1631/jzus.A1500034

Li XZ, Qi CZ, Shao ZS, et al., 2018. Static shear fracture influenced by historic stresses path and crack geometries in brittle solids. *Theoretical and Applied Fracture Mechanics*, 96:64-71. https://doi.org/10.1016/j.tafmec.2018.04.002

Liu N, Zhang CS, Shan ZG, et al., 2019. Deep buried large and long tunnel supporting design and engineering practice under the risk of rock burst. *Chinese Journal of Rock Mechanics and Engineering*, 38(S1):2934-2943 (in Chinese). https://doi.org/10.13722/j.cnki.jrme.2018.1086

Liu Y, Dai F, 2021. A review of experimental and theoretical research on the deformation and failure behavior of rocks subjected to cyclic loading. *Journal of Rock Mechanics and Geotechnical Engineering*, 13(5):1203-1230. https://doi.org/10.1016/j.jrmge.2021.03.012

Morgan SP, Johnson CA, Einstein HH, 2013. Cracking processes in Barre granite: fracture process zones and crack coalescence. *International Journal of Fracture*, 180(2): 177-204. https://doi.org/10.1007/s10704-013-9810-y

Nur A, 1971. Effects of stress on velocity anisotropy in rocks with cracks. *Journal of Geophysical Research: Solid Earth*, 76(8):2022-2034. https://doi.org/10.1029/JB076i008p02022

Peng J, Rong G, Zhou CB, et al., 2016. A study of crack closure effect of rocks and its quantitative model. *Rock and Soil Mechanics*, 37(1):126-132 (in Chinese). https://doi.org/10.16285/j.rsm.2016.01.015

Taheri A, Zhang YB, Munoz H, 2020. Performance of rock crack stress thresholds determination criteria and investigating strength and confining pressure effects. *Construction and Building Materials*, 243:118263. https://doi.org/10.1016/j.conbuildmat.2020.118263

Wang ZL, Feng CC, Wang JG, et al., 2022. An improved statistical damage constitutive model for rock considering the temperature effect. *International Journal of Geomechanics*, 22(11):1-9. https://doi.org/10.1061/(ASCE)GM.1943-5622.0002571

Xie HP, 2019. Research review of the state key research development program of China: deep rock mechanics and mining theory. *Journal of China Coal Society*, 44(5):1283-1305 (in Chinese). https://doi.org/10.13225/j.cnki.jccs.2019.6038

Xie SJ, Han ZY, Lin H, 2022. A quantitative model considering crack closure effect of rock materials. *International Journal of Solids and Structures*, 251:111758. https://doi.org/10.1016/j.ijsolstr.2022.111758

Zhang C, Chen QN, Yang QJ, et al., 2020. Whole process simulation method of brittle rocks deformation and failure considering initial voids closure and its influence. *Journal of China Coal Society*, 45(3):1044-1052 (in Chinese). https://doi.org/10.13225/j.cnki.jccs.2019.0221

Zhang QB, Zhao J, 2014. A review of dynamic experimental techniques and mechanical behaviour of rock materials. *Rock Mechanics and Rock Engineering*, 47(4):1411-1478. https://doi.org/10.1007/s00603-013-0463-y

Zhao Y, Liu HH, 2012. An elastic stress–strain relationship for porous rock under anisotropic stress conditions. *Rock Mechanics and Rock Engineering*, 45(3):389-399. https://doi.org/10.1007/s00603-011-0193-y

Zhou HW, Wang ZH, Ren WG, et al., 2019. Acoustic emission based mechanical behaviors of Beishan granite under conventional triaxial compression and hydro-mechanical coupling tests. *International Journal of Rock Mechanics and Mining Sciences*, 123:104125. https://doi.org/10.1016/j.ijrmms.2019.104125

Zuo JP, Chen Y, Liu XL, 2019. Crack evolution behavior of rocks under confining pressures and its propagation model before peak stress. *Journal of Central South University*, 26(11):3045-3056. https://doi.org/10.1007/s11771-019-4235-z

Electronic supplementary materials

Sections S1–S3, Eqs. (S1)–(S6), Table S1, Figs. S1–S3